

Effect of Top Al₂O₃ Interlayer Thickness on Memory Window and Reliability of FeFETs With TiN/Al₂O₃/Hf_{0.5}Zr_{0.5}O₂/SiO_x/Si (MIFIS) Gate Structure

Tao Hu, Xinpei Jia, Runhao Han, Jia Yang, Mingkai Bai, Saifei Dai, Zeqi Chen, Yajing Ding, Shuai Yang, Kai Han, Yanrong Wang, Jing Zhang, Yuanyuan Zhao, Xiaoyu Ke, Xiaoqing Sun, Junshuai Chai, Hao Xu, Xiaolei Wang, Wenwu Wang and Tianchun Ye

Abstract—We investigate the effect of top Al₂O₃ interlayer thickness on the memory window (MW) of Si channel ferroelectric field-effect transistors (Si-FeFETs) with TiN/Al₂O₃/Hf_{0.5}Zr_{0.5}O₂/SiO_x/Si (MIFIS) gate structure. We find that the MW first increases and then remains almost constant with the increasing thickness of the top Al₂O₃. The phenomenon is attributed to the lower electric field of the ferroelectric Hf_{0.5}Zr_{0.5}O₂ in the MIFIS structure with a thicker top Al₂O₃ after a program operation. The lower electric field makes the charges trapped at the top Al₂O₃/Hf_{0.5}Zr_{0.5}O₂ interface, which are injected from the metal gate, cannot be retained. Furthermore, we study the effect of the top Al₂O₃ interlayer thickness on the reliability (endurance characteristics and retention characteristics). We find that the MIFIS structure with a thicker top Al₂O₃ interlayer has poorer retention and endurance characteristics. Our work is helpful in deeply understanding the effect of top interlayer thickness on the MW and reliability of Si-FeFETs with MIFIS gate stacks.

Index Terms—Memory window (MW), FeFETs, retention, endurance, Hf_{0.5}Zr_{0.5}O₂, MIFIS gate structure.

This work was supported in part by the National Natural Science Foundation of China under Grant Nos. 92264104 and 52350195, in part by National Key Research and Development Program of China under Grant No. 2022YFB4400300, in part by R&D Program of Beijing Municipal Education Commission under Grant No. KZ202210009014, in part by the Young Elite Scientists Sponsorship Program under Grant No. BYESS2023033, and Supported by the Postdoctoral Fellowship Program of CPSF under Grant No. GZC20232925. (Corresponding author: Xiaolei Wang, Hao Xu)

Tao Hu, Xinpei Jia, Runhao Han, Jia Yang, Mingkai Bai, Saifei Dai, Zeqi Chen, Yajing Ding, Shuai Yang, Yuanyuan Zhao, Xiaoyu Ke, Xiaoqing Sun, Junshuai Chai, Hao Xu, Xiaolei Wang, Wenwu Wang and Tianchun Ye are with Institute of Microelectronics of the Chinese Academy of Sciences, Beijing 100029, China. The authors are also with the School of Integrated Circuits, University of Chinese Academy of Sciences, Beijing 100049, China (e-mail: wangxiaolei@ime.ac.cn, xuhao@ime.ac.cn).

Yanrong Wang and Jing Zhang are with School of Information Science and Technology, North China University of Technology, Beijing 100144, China.

Kai Han is with the School of Physics and Electronic Information, Weifang University, Weifang, Shandong 261061, China.

I. INTRODUCTION

The massive data storage market is dominated by NAND flash memory. The primary drivers of NAND flash technology development are density and cost per bit [1]. To meet the growing demand for high-density storage, 3D vertical NAND (3D VNAND) has replaced 2D NAND [2]. However, due to the strong cell-to-cell interference under the high operation voltages, 3D VNAND currently faces scaling limits in the Z-direction [1, 3, 4]. Ferroelectric-based vertical NAND (Fe-VNAND) is one of the strong candidates for 3D VNAND technology to overcome the scaling limits [1, 3-7]. However, Fe-VNAND faces the huge challenge of a narrow memory window (MW) for the application in high-density storage. Generally, hafnia-based silicon channel ferroelectric field-effect transistors (HfO₂-based Si-FeFETs) with metal/HfO₂-based ferroelectric/bottom interlayer/silicon substrate (MFIS) gate structure has a MW of about 1-2 V [8-11]. The physical origin of narrow MW are low coercive voltage (V_c) of ferroelectric Hf_{0.5}Zr_{0.5}O₂ within the thickness range of 20 nm, and a significant charge trapping effect between the silicon channel and ferroelectric Hf_{0.5}Zr_{0.5}O₂/SiO_x interface due to the presence of the large spontaneous polarization (P_s) of ferroelectric doped-HfO₂ (~ 20 -30 $\mu\text{C}/\text{cm}^2$) [12-15]. However, the coercive field of the ferroelectric Hf_{0.5}Zr_{0.5}O₂ is difficult to change on a large range. Therefore, to enlarge the MW, several studies focus on suppressing the charge injection from the silicon channel to the ferroelectric Hf_{0.5}Zr_{0.5}O₂/SiO_x interface, such as reducing the spontaneous polarization of the ferroelectric [16-19], eliminating the bottom interlayer [20-24], and applying high- κ interlayer [25-29]. However, the above methods still cannot significantly enlarge the MW. This small MW does not meet the requirements of the multi-bit memory cell. Recently, some studies have found that inserting a dielectric interlayer (e.g. Al₂O₃ or SiO₂) between the metal gate and the ferroelectric layer can significantly improve the MW of Si-FeFETs [1, 3, 4, 24, 30-35]. The MW can achieve 6.4 V (or 8.3 V) by inserting 3.4 nm (or 4 nm) SiO₂ and 4.1 V by inserting 3 nm Al₂O₃ [32, 33, 35]. Moreover, the simulation

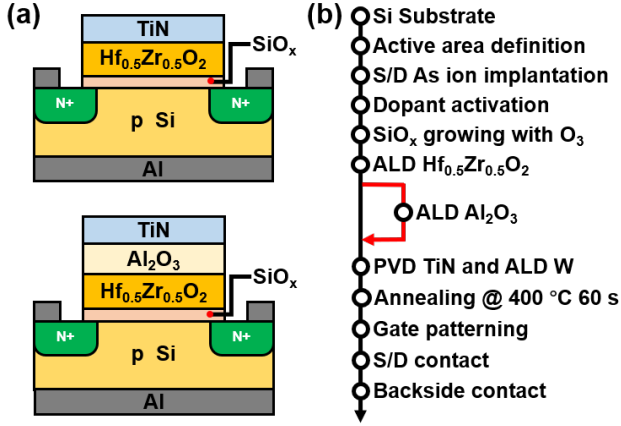


Fig. 1. (a) Schematic of the HfO₂-based Si-FeFETs device structure and (b) fabrication process flow.

results from [1] show that using a thicker top interlayer is beneficial for the MW increase.

However, there are still few experimental studies on the effect of the top Al₂O₃ interlayer thickness on the MW and reliability of Si-FeFETs. Therefore, we experimentally study and report the dependence of the MW and reliability on the top Al₂O₃ interlayer thickness and discuss its physical origin in this work. We find that the MW first increases and then remains almost constant with the increasing thickness of the top Al₂O₃. The phenomenon is attributed to the lower electric field of the ferroelectric Hf_{0.5}Zr_{0.5}O₂ in the MIFIS structure with a thicker top Al₂O₃ after a program operation. The lower electric field makes the charges trapped at the top Al₂O₃/Hf_{0.5}Zr_{0.5}O₂ interface (Q_{it}), which are injected from the metal gate, cannot be retained. Furthermore, we study the effect of the top Al₂O₃ interlayer thickness on the reliability (endurance characteristics and retention characteristics). We find that the MIFIS structure with a thicker top Al₂O₃ interlayer has poorer retention characteristics and endurance characteristics.

II. DEVICE FABRICATION AND CHARACTERIZATION

Fig. 1 shows the schematic of the HfO₂-based Si-FeFETs device structure and fabrication process flow. In our work, there are two different gate stacks. One is TiN/Hf_{0.5}Zr_{0.5}O₂/SiO_x/Si (MFIS) as the control sample. The other is TiN/Al₂O₃/Hf_{0.5}Zr_{0.5}O₂/SiO_x/Si (MIFIS) with a 0.85, 1.7, 2.55, 4.5, 5.5, 8, or 13 nm top Al₂O₃ dielectric interlayer. The detailed fabrication procedure of these devices can be found in the previous report [32].

Fig. 2 shows High-Resolution Transmission Electron Microscopy (HRTEM) images and Energy Dispersion Spectrometer (EDS) results for both MFIS and MIFIS structures, where the MIFIS structure with 4.5 nm top Al₂O₃ interlayer is shown as an example of the MIFIS structure with different top Al₂O₃ thicknesses. For the MIFIS structure, the presence of a peak concentration of Al at the TiN/Hf_{0.5}Zr_{0.5}O₂ interface confirms the presence of the top Al₂O₃ interlayer.

The gate length/width (L/W) of these devices in this work is 5/150 μm. The electrical measurements were performed by Keysight B1500A with waveform generator fast measurement unit (WGFMU) and high voltage semiconductor pulse

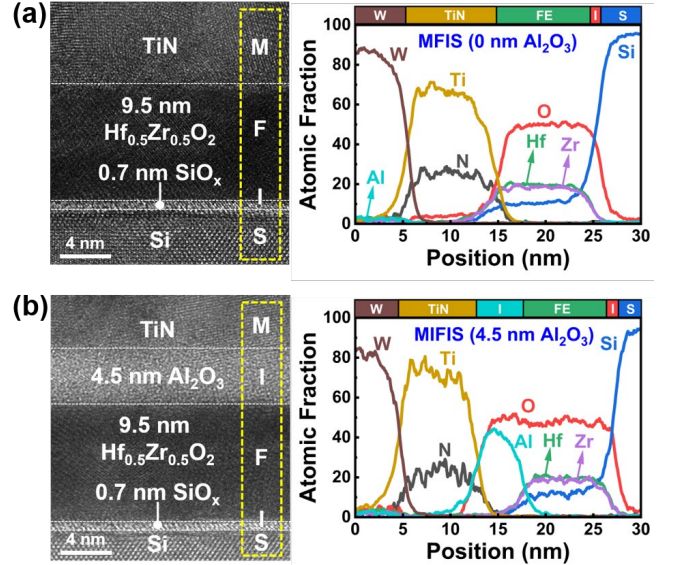


Fig. 2. HRTEM images and EDS of the (a) MFIS and (b) MIFIS structures with 4.5 nm top Al₂O₃ interlayer.

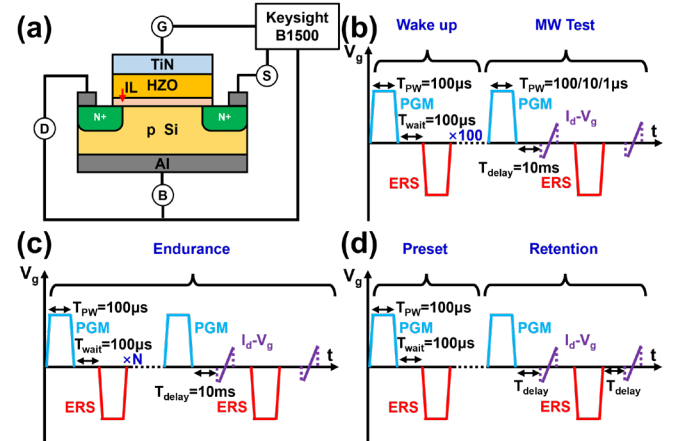


Fig. 3. (a) Schematic of electrical measurement of these devices. The measurement waveforms of (b) MW, (c) endurance characteristics and (d) retention characteristics.

generator unit (SPGU). Fig. 3(a) shows the schematic of the electrical measurement of these devices. Fig. 3(b-d) shows the measurement waveforms of MW, endurance characteristics, and retention characteristics. The threshold voltage (V_{th}) is extracted by the constant current method at the drain current $I_d = W/L \times 10^{-7}$ A.

III. MODEL

For the MIFIS gate structure as shown in Fig. 1(a), the voltage distribution across the gate stacks is given as

$$V_g = \phi_s + V_{FE} + V_{BIL} + V_{TIL} \quad (1)$$

where V_g is the gate voltage, ϕ_s , V_{FE} , V_{BIL} , and V_{TIL} are the voltage drop across Si substrate, ferroelectric Hf_{0.5}Zr_{0.5}O₂, bottom SiO_x interlayer, and top Al₂O₃ interlayer, respectively. The work function difference between the metal gate and the Si substrate is set to zero here. According to the charge neutrality condition, we can obtain

$$Q_M + Q_{it'} + Q_{it} + Q_s = 0 \quad (2)$$

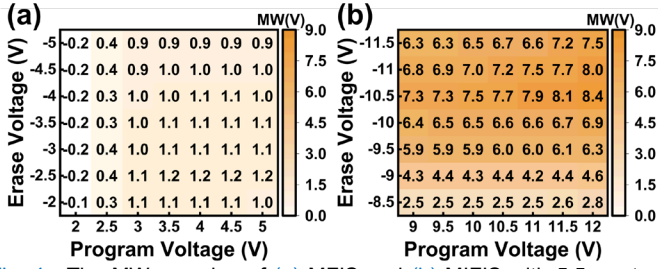


Fig. 4. The MW mapping of (a) MFIS and (b) MIFIS with 5.5 nm top Al₂O₃ as a function of the pulse amplitude under the pulse width of 100 μ s.

where Q_M , Q_{it} , $Q_{it'}$, and Q_s are the charge density of the metal gate, bottom SiO_x/Hf_{0.5}Zr_{0.5}O₂ interface, top Al₂O₃/Hf_{0.5}Zr_{0.5}O₂ interface, and Si substrate, respectively. V_{TIL} is given as

$$V_{TIL} = \frac{Q_M}{C_{TIL}} \quad (3)$$

where C_{TIL} is the capacitance of the top Al₂O₃ interlayer. V_{BIL} is given as

$$V_{BIL} = \frac{-Q_{Si}}{C_{BIL}} = \frac{Q_M + Q_{it'} + Q_{it}}{C_{BIL}} \quad (4)$$

where C_{BIL} represents the capacitance of the bottom SiO_x interlayer. The relationship between the charge density of the Si substrate Q_s and the Si surface potential ϕ_s is given by [11]

$$\begin{aligned} Q_s(\phi_s) &= -SGN(\phi_s) \sqrt{2}(\epsilon_0 \epsilon_s / \beta L_D) \\ &\quad \times ((e^{-\beta \phi_s} + \beta \phi_s - 1) + (\frac{n_i}{N_a})^2 (e^{\beta \phi_s} - \beta \phi_s - 1))^{\frac{1}{2}} \end{aligned} \quad (5)$$

where $\beta = q/(kT)$, $L_D = (\epsilon_0 \epsilon_s / q \beta N_a)$, ϵ_0 is the vacuum dielectric constant, ϵ_s is the relative dielectric constant of the silicon, n_i is the intrinsic carrier concentration of the silicon, and N_a is the substrate doping concentration.

Introducing (3) and (4) into (1), the expression of the load line for the MIFIS structure is given as

$$Q_M + Q_{it'} = \frac{C_{TIL} C_{BIL}}{C_{TIL} + C_{BIL}} (V_g - V_{FE} - \phi_s + \frac{Q_{it'} + Q_{it}}{C_{TIL}}) - Q_{it} \quad (6)$$

According to (5), we find that the distance that the load line shifts up and down depends on the amount of the Q_{it} trapped at the bottom SiO_x/Hf_{0.5}Zr_{0.5}O₂ interface, while $Q_{it} + Q_{it'}$ and C_{TIL} determine the distance that the curve shifts left and right.

Based on the principle of the continuity of the electric displacement vector, $Q_M + Q_{it'}$ can be expressed as

$$Q_M + Q_{it'} = C_{FE} V_{FE} + P(V_{FE}) \quad (7)$$

where C_{FE} is the background capacitance of the ferroelectric Hf_{0.5}Zr_{0.5}O₂. The ferroelectric hysteresis loop is obtained by adopting the Preisach model here [36]

$$P(V_{FE}) = P_s \tanh[\alpha(V_{FE} \pm V_C)] \quad (8)$$

where P_s is the saturation polarization, V_C is the coercive voltage, and α is a constant describing how fast the hyperbolic tangent approaches $\pm P_s$. Solve (6), (7), and (8) simultaneously, the distribution of voltage and charge of the MIFIS gate stacks at each gate voltage can be obtained by combining the hysteresis loop and the load line.

In simulation, the doping concentration of the silicon substrate is set as 10^{17} cm⁻³. The physical thicknesses of ferroelectric Hf_{0.5}Zr_{0.5}O₂ and bottom SiO_x interlayer are 9.5 nm

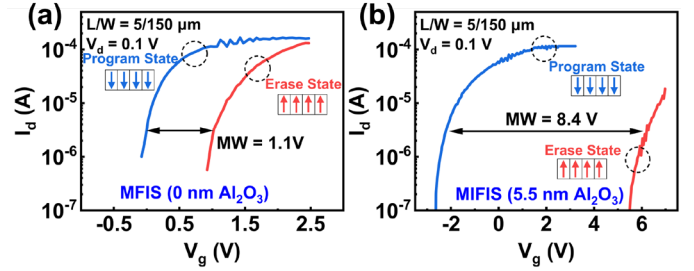


Fig. 5. I_d - V_g curves of the maximum MW for (a) MFIS and (b) MIFIS with 5.5 nm top Al₂O₃ interlayer under the pulse width of 100 μ s.

and 0.7 nm, respectively. The relative dielectric constant of the ferroelectric Hf_{0.5}Zr_{0.5}O₂, top Al₂O₃ interlayer, and bottom SiO_x interlayer is 30, 9, and 3.9, respectively. For the ferroelectric Hf_{0.5}Zr_{0.5}O₂, the saturated polarization (P_s) is set as 23 μ C/cm², and the remanent polarization (P_r) is set as 20 μ C/cm². The coercive field is set as 1.5 mV/cm.

IV. RESULTS AND DISCUSSIONS

A. The effect of the top Al₂O₃ interlayer thickness on the MW

We investigate the dependence of the MW on the pulse amplitude. Fig. 4(a) and (b) show the MW mapping results for the MFIS structure and MIFIS structure with the 5.5 nm top Al₂O₃ interlayer under the pulse width of 100 μ s. For the MFIS structure and MIFIS structure with the 5.5 nm top Al₂O₃, when the program pulse amplitude goes beyond 5 V or 12 V under the pulse width of 100 μ s, respectively, the devices break down. Thus, the maximum MW is 8.4 V for the MIFIS structure with the 5.5 nm top Al₂O₃ interlayer, while the maximum MW is 1.2 V for the MFIS structure. This indicates that the top Al₂O₃ interlayer between the metal gate TiN and ferroelectric Hf_{0.5}Zr_{0.5}O₂ can significantly improve the MW. Fig. 5(a) and (b) show the I_d - V_g curves corresponding to the maximum MW for the MFIS structure and MIFIS structure with 5.5 nm top Al₂O₃ interlayer, respectively.

We repeated the above MW mapping measurement process under different pulse widths (not shown here). The maximum MW that can be achieved under different pulse widths is equal to that obtained under the pulse width of 100 μ s, as described in [32]. Thus, the pulse width does not affect the above conclusion that the top dielectric between the ferroelectric and the metal gate can significantly increase the MW of the Si-FeFETs.

We study the effect of the top Al₂O₃ interlayer thickness on the maximum MW. For each sample, we repeated the above MW mapping measurement process. Fig. 6(a) shows the dependence of the maximum MW on the top Al₂O₃ interlayer thickness. Fig. 6(b) shows the dependence of the V_{th} corresponding to the maximum MW on the top Al₂O₃ interlayer thickness. We find that the maximum MW first increases at stage I and then remains almost constant at stage II as the thickness of the top Al₂O₃ interlayer increases. We will discuss its physical origin subsequently.

B. The physical origin of the dependence of maximum MW on the top Al₂O₃ interlayer thickness

We discuss the physical origin of the dependence of maximum MW on the top Al₂O₃ thickness in stages I and II,

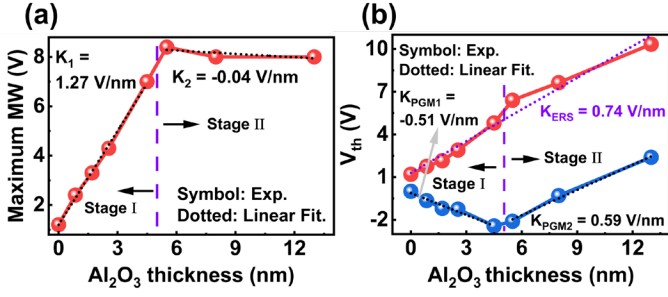


Fig. 6. The dependence of (a) the maximum MW and (b) the V_{th} corresponding to the maximum MW on the top Al_2O_3 interlayer thickness.

respectively. Firstly, we discuss the physical origin of the dependence of the maximum MW on the top Al_2O_3 interlayer thickness at stage I as shown in Fig. 6(a). The physical origin of the MW enlargement by inserting the top Al_2O_3 interlayer is attributed to the presence of the charges injected from the metal gate trapped at the top $\text{Al}_2\text{O}_3/\text{Hf}_{0.5}\text{Zr}_{0.5}\text{O}_2$ interface (Q_{it}), as described at [1, 24, 32]. During the program operation, electron de-trapping and/or hole trapping at the top $\text{Al}_2\text{O}_3/\text{Hf}_{0.5}\text{Zr}_{0.5}\text{O}_2$ interface occurs due to the downward movement of the Fermi energy of the metal gate. After the program operation, positive charges are trapped at the top $\text{Al}_2\text{O}_3/\text{Hf}_{0.5}\text{Zr}_{0.5}\text{O}_2$ interface because the top Al_2O_3 acts as a barrier layer. Then the V_{th} after program operation ($V_{th,PGM}$) negatively shifts. Similarly, after the erase operation, negative charges are trapped at the same interface, causing a positive shift of the $V_{th,ERS}$. The shift of the threshold voltage of the MIFIS structure compared with that of the MFIS structure (ΔV_{th}) is calculated by

$$\Delta V_{th} \approx -\frac{(Q_{it}^+ + Q_{it}^-)}{\epsilon_0 \epsilon_{\text{AlO}_3}} d_{\text{AlO}_3} \quad (9)$$

where ϵ_{AlO_3} and d_{AlO_3} are the relative dielectric constant and physical thickness of the top Al_2O_3 interlayer, respectively. For the MFIS and MIFIS structures, the Q_{it} is identical due to the same bottom SiO_x interlayer. According to (9), the linear dependence of the $V_{th,PGM}$ (or $V_{th,ERS}$) on the top Al_2O_3 thickness at stage I indicates that the positive (or negative) charges Q_{it} after the program (or erase) operation remains constant in the MIFIS structure with different thickness, which is consistent with the description at [1, 35]. Finally, the above results lead to a linear dependence of the maximum MW vs. top Al_2O_3 thickness at stage I. Furthermore, the absolute value of the slope of linear dependence corresponding to the program operation is less than that of linear dependence corresponding to the erase operation. This shows that the net number of the positive charges after the program operation is less than the net number of the negative charges after the erase operation according to (9) (the net number of the charges is the sum of the charges trapped at the top $\text{Al}_2\text{O}_3/\text{Hf}_{0.5}\text{Zr}_{0.5}\text{O}_2$ interface and bottom $\text{SiO}_x/\text{Hf}_{0.5}\text{Zr}_{0.5}\text{O}_2$ interface).

Secondly, we discuss the physical origin of the dependence of the maximum MW and V_{th} on the top Al_2O_3 interlayer thickness at stage II. As shown in stage I, the $V_{th,ERS}$ still increases linearly with the Al_2O_3 interlayer thickness at stage II, which means the Q_{it} after the erase operation is identical in the MIFIS structure with different top Al_2O_3 thicknesses. However, we find that the $V_{th,PGM}$ no longer decreases linearly with the top

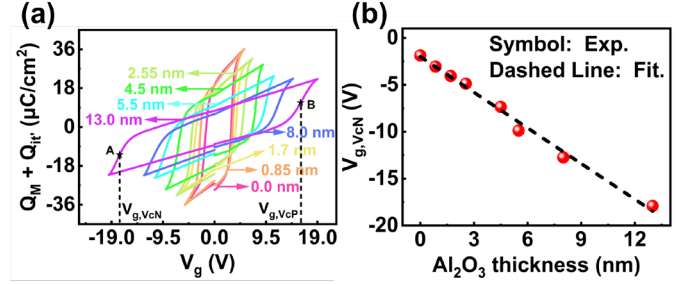


Fig. 7. (a) Results of the PV measurement. (b) The dependence of $V_{g,VcN}$ on the physical thickness of top Al_2O_3 interlayer.

Al_2O_3 interlayer thickness as that in stage I, which results in the maximum MW remaining almost constant with the increasing thickness of the top Al_2O_3 interlayer at stage II.

We discuss the physical origin of the fact that $V_{th,PGM}$ does not decrease linearly with the increasing thickness of top Al_2O_3 at stage II. According to (9), the dependence of the $V_{th,PGM}$ on the top Al_2O_3 thickness at stage II indicates the presence of $Q_{it}^- < |Q_{it}^+|$. Therefore, the reduction in Q_{it}^- results in the dependence of the $V_{th,PGM}$ on the top Al_2O_3 thickness at stage II. The reduction in Q_{it}^- after the program operation may be caused by the two reasons as follows: (i) As the thickness of the top Al_2O_3 increases, the hole trapping and/or electron de-trapping at the top $\text{Al}_2\text{O}_3/\text{Hf}_{0.5}\text{Zr}_{0.5}\text{O}_2$ interface may be more difficult to occur during the program operation due to an increase in the tunneling potential barrier, which may result in the reduction in Q_{it}^- during the program operation. (ii) The retention capability of the charges Q_{it}^- injected during the program operation degrades rapidly with increasing thickness of the top Al_2O_3 , leading to a reduction in Q_{it}^- before the V_{th} is measured. We discuss their reasonableness in detail as follows.

To investigate whether the charges (Q_{it}) are fully injected during the program operation, we conducted the PV measurement for these devices to obtain the I_g - V_g curves. Fig. 7(a) shows the measurement results obtained by integrating the I_g . Fig. 7(a) shows that: (i) the slope of the linear part of the total charge density vs. gate voltage ($Q_M + Q_{it} - V_g$) curves decreases with increasing thickness of the top Al_2O_3 , which is attributed to the equivalent gate capacitance decreases with the increasing thickness of top Al_2O_3 . (ii) The intersections of the $Q_M + Q_{it} - V_g$ curves and the V_g axis become closer to the linear part of the $Q_M + Q_{it} - V_g$ curves as the thickness of the top Al_2O_3 increases. This is caused by a decrease in the measured polarization value. (iii) the $Q_M + Q_{it} - V_g$ curves broaden with increasing thickness of the top Al_2O_3 . Our measurement results are similar to [1]. The physical origin of the broadener of the $Q_M + Q_{it} - V_g$ curves is attributed to the partial voltage across the top Al_2O_3 interlayer caused by the hysteresis of the charges Q_{it} . Therefore, the degree to which the $Q_M + Q_{it} - V_g$ curves broaden can represent the number of charges trapped at the top $\text{Al}_2\text{O}_3/\text{Hf}_{0.5}\text{Zr}_{0.5}\text{O}_2$ interface. To more reasonably evaluate the degree of broadening of the $Q_M + Q_{it} - V_g$ curves, we use the voltage value where the ferroelectric polarization switching rate is 50% to evaluate, such as points A and B shown in Fig. 7(a). Fig. 8(b) shows that gate voltage ($V_{g,VcN}$) corresponding to ferroelectric negative coercive voltage is linearly dependent on the top Al_2O_3 interlayer thickness, which indicates the Q_{it} after the program operation is identical for the MIFIS structure with different top Al_2O_3 thicknesses. Therefore, the dependence of

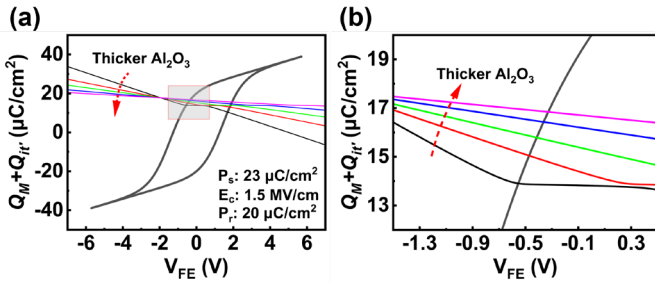


Fig. 8. (a) Hysteresis loop of $Q_M + Q_{it} - V_{FE}$ and load line at $V_g = 0$ V after the program operation for the different top Al₂O₃ thicknesses. (b) Enlarged view of the box section in (a).

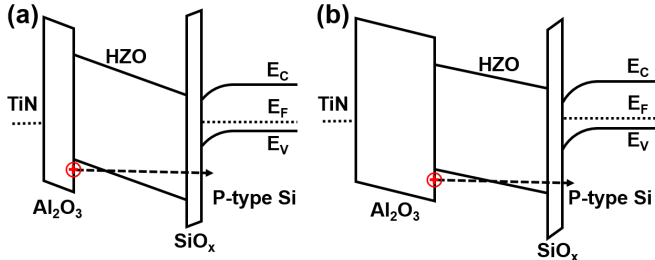


Fig. 9. Energy band diagrams for the MIFIS structure with (a) a thinner Al₂O₃ and (b) a thicker Al₂O₃ interlayer at $V_g = 0$ V after the program operation.

the $V_{th,PGM}$ on the top Al₂O₃ interlayer thickness at stage II is attributed to the reduction in Q_{it} caused by the retention degradation.

We use the load line and the ferroelectric hysteresis loop to further explain the physical origin of the retention degradation. We consider the charge trapping phenomenon at the Al₂O₃/Hf_{0.5}Zr_{0.5}O₂ interface and the bottom SiO_x/Hf_{0.5}Zr_{0.5}O₂ interface. Recent research work shows that the charge density trapped at the bottom SiO_x/Hf_{0.5}Zr_{0.5}O₂ interface after the program operation is about $-13.0 \mu\text{C}/\text{cm}^2$, while the trapped charge density after the erase operation is only about $2.6 \mu\text{C}/\text{cm}^2$ [37]. According to (9) as well as Fig. 6(b), the value Q_{it} after the program and erase operation is set as $17.7 \mu\text{C}/\text{cm}^2$ and $-8.5 \mu\text{C}/\text{cm}^2$, respectively. In simulation, the doping concentration of the silicon substrate is set as 10^{17}cm^{-3} . The physical thicknesses of ferroelectric Hf_{0.5}Zr_{0.5}O₂ and bottom SiO_x interlayer are 9.5 nm and 0.7 nm, respectively. The relative dielectric constant of the ferroelectric Hf_{0.5}Zr_{0.5}O₂ and top Al₂O₃ is 30 and 9, respectively. Furthermore, since we are considering the effect of the top Al₂O₃ interlayer thickness on the maximum MW of the FeFETs with MIFIS structure, i.e., the gate voltage is large enough, we use the saturation hysteresis loop in the simulation.

We conduct the simulation at $V_g = 0$ V after the program operation. Fig. 8(a-b) shows the hysteresis loop of $Q_M + Q_{it} - V_{FE}$ and load line at $V_g = 0$ V after the program operation for different top Al₂O₃ thicknesses. We find that the electric field of the ferroelectric Hf_{0.5}Zr_{0.5}O₂ gradually decreases with increasing thickness of the top Al₂O₃ as shown in the Fig. 8(b). This means that the charges Q_{it} face a smaller tunneling potential barrier for the MIFIS structure with a thicker top Al₂O₃ when Q_{it} tunnel to the Si substrate, as shown in Fig. 9, which results in more charges Q_{it} tunneling to the Si substrate to recombine with electrons. The above result leads to a

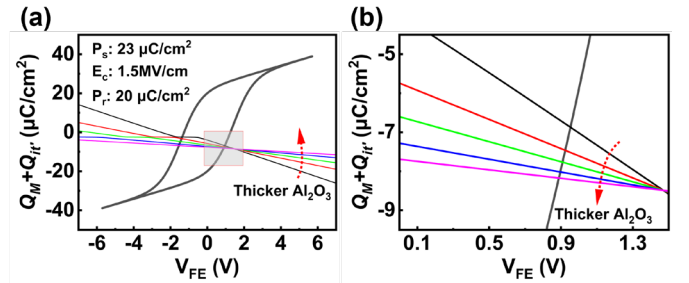


Fig. 10. (a) Hysteresis loop of $Q_M + Q_{it} - V_{FE}$ and load line at $V_g = 0$ V after the erase operation for the different top Al₂O₃ thicknesses. (b) Enlarged view of the box section in (a).

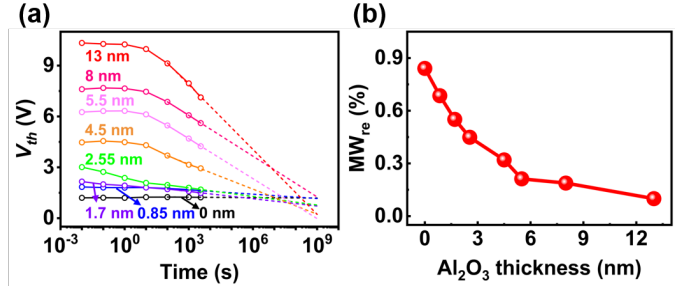


Fig. 11. (a) Retention characteristics after the erase operation for the MIFIS structures with different top Al₂O₃ thicknesses. (b) The dependence of the MW retention ratio (MW_{re}) on the top Al₂O₃ interlayer thickness.

decrease in Q_{it} , so that Q_{it} becomes less than $|Q_{it}|$ ($Q_{it} < |Q_{it}|$) after the program operation in the MIFIS structure with a thicker top Al₂O₃ interlayer. Therefore, the $V_{th,PGM}$ no longer decreases linearly with increasing thickness of the top Al₂O₃ interlayer at stage II.

In addition, we perform the simulation at $V_g = 0$ V after the erase operation to further discuss the reason why the charge trapped at the top Al₂O₃/Hf_{0.5}Zr_{0.5}O₂ interface (Q_{it}) after the erase operation can be maintained. Fig. 10 shows the hysteresis loop of $Q_M + Q_{it} - V_{FE}$ and load line at $V_g = 0$ V after the erase operation for the different top Al₂O₃ thicknesses. According to (6), we find that compared with the program operation, the load line shifts downward by a smaller distance due to the smaller charge density trapped at the bottom SiO_x/Hf_{0.5}Zr_{0.5}O₂ interface (Q_{it}) after the erase operation. Therefore, the change in the electric field of the ferroelectric Hf_{0.5}Zr_{0.5}O₂ after the erase operation caused by the change in thickness of the top Al₂O₃ interlayer is reduced. This indicates that there is only a slight difference in tunneling potential barriers faced by Q_{it} in the MIFIS structure with different Al₂O₃ thicknesses. The slight difference does not cause a significant decrease in Q_{it} within a short time. Thus, the $V_{th,ERS}$ is linearly dependent on the thickness of the top Al₂O₃ interlayer over the entire thickness range.

C. The effect of top Al₂O₃ thickness on the endurance and retention characteristics

We investigate the dependence of the retention characteristics under the pulse amplitude corresponding to the maximum MW on top Al₂O₃ interlayer thicknesses. Fig. 11(a) shows the retention characteristic after the erase operation for the MIFIS structures with different top Al₂O₃ interlayer thicknesses. We find that the $V_{th,ERS}$ first remains almost

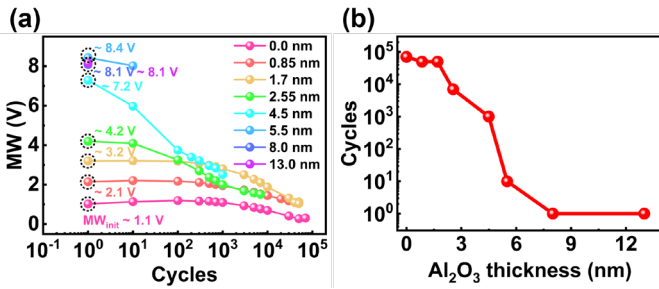


Fig. 12. (a) Endurance characteristics corresponding to the maximum MW. (b) The dependence of the cycles that correspond to the device endurance failure on the top Al₂O₃ interlayer thickness.

constant within a time range of 10 s and then decreases with an increase in time. In addition, this degradation rate of $V_{th,ERS}$ increases with the increasing thickness of the top Al₂O₃ interlayer.

We discuss the physical origin of the dependence of the retention characteristics after the erase operation on top Al₂O₃ thickness. As the above discussion, the electric field of the ferroelectric Hf_{0.5}Zr_{0.5}O₂ after the erase operation decreases as the thickness of the top Al₂O₃ increases, as shown in Fig. 10. This leads to the fact that the degradation rate of the $V_{th,ERS}$ increases with the increasing thickness of the top Al₂O₃ interlayer. In addition, on the whole, the electric field of the ferroelectric Hf_{0.5}Zr_{0.5}O₂ only exhibits a slight difference for the different thicknesses of the top Al₂O₃. The slight difference in the electric field results in a slight difference in tunneling potential barriers. Nevertheless, the slight difference of tunneling potential barriers does not cause a significant decrease in Q_{it} within a short time, Thus, the $V_{th,ERS}$ remains almost constant within a time range of 10 s for the different top Al₂O₃ interlayer thicknesses.

We define the ratio of the MW_{end} (delay = 3.15×10^8 s) to the MW_{init} (delay = 10 ms) as the MW retention ratio (MW_{re}), i.e.,

$$MW_{re} = \frac{MW_{end}}{MW_{init}} \quad (9)$$

Fig. 11(b) shows the dependence of the MW_{re} on the top Al₂O₃ interlayer thickness. We find the MW_{re} decreases with the increasing thickness of the top Al₂O₃ interlayer. This indicates the MIFIS structure with a thicker top Al₂O₃ has poorer retention characteristics. The retention characteristics after the program operation exhibit little difference compared with those of the erase operation (not shown here), and therefore, the above phenomenon is attributed to the dependence of the degradation rate of the $V_{th,ERS}$ on the thickness of the top Al₂O₃ interlayer.

Furthermore, we study the impact of top Al₂O₃ interlayer thickness on the endurance characteristics under the pulse amplitude of the corresponding maximum MW. Fig. 13(a) shows the measurement results of endurance characteristics corresponding to the maximum MW. We define the cycles corresponding to MW = 0 or breakdown failure of gate stacks as the endurance failure cycles of the device. Fig. 13(b) shows the dependence of the endurance failure cycles on the top Al₂O₃ interlayer thickness. We find the MIFIS with a thicker top Al₂O₃ dielectric interlayer has poorer endurance characteristics, which is similar to the degradation of the endurance characteristics with the increasing thickness of the top SiO₂

interlayer described in [35]. The possible physical origin is the breakdown of the top Al₂O₃ dielectric interlayer. Since the rate of ferroelectric polarization switching is higher than the rate of charge trapping and de-trapping [14, 37-39]. Therefore, the ferroelectric polarization switches in a shorter time after the application of the program pulse, and the large spontaneous polarization (P_s) of ferroelectric Hf_{0.5}Zr_{0.5}O₂ leads to an electric field of the top Al₂O₃ that is almost close to its breakdown electric field. However, as the thickness of the top Al₂O₃ interlayer increases, the time that the same amount of charge is injected from the metal gate to the top Al₂O₃/Hf_{0.5}Zr_{0.5}O₂ interface (Q_{it}) increases. This indicates that the thicker top Al₂O₃ dielectric interlayer experiences a longer time at a high electric field. In addition, some studies have shown that the dielectric breakdown strength (E_{bd}) reduces as the dielectric thickness increases [40]. Thus, the MIFIS structure with a thicker top Al₂O₃ interlayer is more susceptible to breakdown under pulse amplitude corresponding to maximum MW. This leads to the phenomenon that the endurance characteristics deteriorate with increasing thickness of the top Al₂O₃ interlayer.

V. CONCLUSIONS

In our work, we study the effect of the top Al₂O₃ interlayer thickness on the MW of FeFETs with the MIFIS gate structure. We find the MW first increases and then remains almost constant with the increasing thickness of the top Al₂O₃. The phenomenon is attributed to the lower electric field of the ferroelectric Hf_{0.5}Zr_{0.5}O₂ in the MIFIS structure with a thicker top Al₂O₃ after a program operation, which makes the charges (Q_{it}) trapped at the top Al₂O₃/Hf_{0.5}Zr_{0.5}O₂ interface cannot be retained. Furthermore, we investigate the effect of the top Al₂O₃ interlayer thickness on the reliability (endurance characteristics and retention characteristics). We find that the MIFIS structure with a thicker top Al₂O₃ interlayer has poorer retention endurance characteristics.

REFERENCES

- [1] S. Lim, T. Kim, I. Myeong, S. Park, S. Noh, S. M. Lee et al., "Comprehensive Design Guidelines of Gate Stack for QLC and Highly Reliable Ferroelectric VNAND," in *IEDM Tech. Dig.*, Dec. 2023, pp. 1-4, doi: 10.1109/IEDM45741.2023.10413820.
- [2] J. Jang, H. S. Kim, W. Cho, H. Cho, K. Jinho, S. I. Shim et al., "Vertical cell array using TCAT(Terabit Cell Array Transistor) technology for ultra high density NAND flash memory," in *Proc. Symp. VLSI Technol.*, Jun. 2009, pp. 192-193, doi.
- [3] I. Myeong, H. Kim, S. Kim, S. Lim, K. Kim, W. Kim et al., "Strategies for a Wide Memory Window of Ferroelectric FET for Multilevel Ferroelectric VNAND Operation," *IEEE Electron Device Lett.*, vol. 45, no. 7, pp. 1185-1188, 2024, doi: 10.1109/LED.2024.3400983.
- [4] S. Yoon, S. I. Hong, D. Kim, G. Choi, Y. M. Kim, K. Min et al., "QLC Programmable 3D Ferroelectric NAND Flash Memory by Memory Window Expansion using Cell Stack Engineering," in *Proc. Symp. VLSI Technol.*, Jun. 2023, pp. 1-2, doi: 10.23919/VLSITechnologyandCir57934.2023.10185294.
- [5] K. Florent, M. Pesic, A. Subirats, K. Banerjee, S. Lavizzari, A. Arreghini et al., "Vertical Ferroelectric HfO₂ FET based on 3D NAND Architecture: Towards Dense Low-Power Memory," in *IEDM Tech. Dig.*, Dec. 2018, pp. 2.5.1-2.5.4, doi: 10.1109/IEDM.2018.8614710.
- [6] S. Yoon, S. I. Hong, G. Choi, D. Kim, I. Kim, S. M. Jeon et al., "Highly Stackable 3D Ferroelectric NAND Devices: Beyond the Charge Trap Based Memory," in *Proc. IEEE Int. Memory Workshop (IMW)*, May 2022, pp. 1-4, doi: 10.1109/IMW52921.2022.9779278.

- [7] K. Florent, S. Lavizzari, L. D. Piazza, M. Popovici, E. Vecchio, G. Potoms et al., "First demonstration of vertically stacked ferroelectric Al doped HfO₂ devices for NAND applications," in *Proc. Symp. VLSI Technol.*, Jun. 2017, pp. T158-T159, doi: 10.23919/VLSIT.2017.7998162.
- [8] H. Mulaosmanovic, E. T. Breyer, T. Mikolajick, and S. Slesazek, "Recovery of Cycling Endurance Failure in Ferroelectric FETs by Self-Heating," *IEEE Electron Device Lett.*, vol. 40, no. 2, pp. 216-219, Feb. 2019, doi: 10.1109/LED.2018.2889412.
- [9] R. Ichihara, K. Suzuki, H. Kusai, K. Ariyoshi, K. Akari, K. Takano et al., "Re-Examination of V_{th} Window and Reliability in HfO₂ FeFET Based on the Direct Extraction of Spontaneous Polarization and Trap Charge during Memory Operation," in *Proc. Symp. VLSI Technol.*, Jun. 2020, pp. 1-2, doi: 10.1109/VLSITechnology18217.2020.9265055.
- [10] D. H. Min, S. Y. Kang, S. E. Moon, and S. M. Yoon, "Impact of Thickness Control of Hf_{0.5}Zr_{0.5}O₂ Films for the Metal-Ferroelectric-Insulator-Semiconductor Capacitors," *IEEE Electron Device Lett.*, vol. 40, no. 7, pp. 1032-1035, May 2019, doi: 10.1109/LED.2019.2917032.
- [11] X. Jia, J. Chai, J. Duan, X. Sun, X. Shao, J. Xiang et al., "Investigation of Charge Trapping Induced Trap Generation in Si FeFET With Ferroelectric Hf_{0.5}Zr_{0.5}O₂," *IEEE Trans. Electron Devices*, vol. 71, no. 3, pp. 1845-1851, Mar. 2024, doi: 10.1109/TED.2024.3351599.
- [12] N. Gong, and T. P. Ma, "A Study of Endurance Issues in HfO₂-Based Ferroelectric Field Effect Transistors: Charge Trapping and Trap Generation," *IEEE Electron Device Lett.*, vol. 39, no. 1, pp. 15-18, Jan. 2018, doi: 10.1109/LED.2017.2776263.
- [13] K. Toprasertpong, Z. Y. Lin, T. E. Lee, M. Takenaka, and S. Takagi, "Asymmetric Polarization Response of Electrons and Holes in Si FeFETs: Demonstration of Absolute Polarization Hysteresis Loop and Inversion Hole Density over $2 \times 10^{13} \text{ cm}^{-2}$," in *Proc. Symp. VLSI Technol.*, Jun. 2020, pp. 1-2, doi: 10.1109/VLSITechnology18217.2020.9265015.
- [14] E. Yurchuk, J. Müller, S. Müller, J. Paul, M. Pešić, R. v. Bentum et al., "Charge-Trapping Phenomena in HfO₂-Based FeFET-Type Nonvolatile Memories," *IEEE Trans. Electron Devices*, vol. 63, no. 9, pp. 3501-3507, Sept. 2016, doi: 10.1109/TED.2016.2588439.
- [15] B. Zeng, M. Liao, J. Liao, W. Xiao, Q. Peng, S. Zheng et al., "Program/Erase Cycling Degradation Mechanism of HfO₂-Based FeFET Memory Devices," *IEEE Electron Device Lett.*, vol. 40, no. 5, pp. 710-713, May 2019, doi: 10.1109/LED.2019.2908084.
- [16] S. Deng, Z. Liu, X. Li, T. P. Ma, and K. Ni, "Guidelines for Ferroelectric FET Reliability Optimization: Charge Matching," *IEEE Electron Device Lett.*, vol. 41, no. 9, pp. 1348-1351, Sept. 2020, doi: 10.1109/LED.2020.3011037.
- [17] T. Kim, J. Hwang, G. Kim, M. Jung, and S. Jeon, "High-Performance and High-Endurance HfO₂-Based Ferroelectric Field-Effect Transistor Memory with a Spherical Recess Channel," *physica status solidi (RRL) – Rapid Research Letters*, vol. 15, no. 5, pp. 2100018, May 2021, doi: 10.1002/pssr.202100018.
- [18] M. Liao, H. Xu, J. Duan, S. Zhao, F. Tian, J. Chai et al., "Impact of Saturated Spontaneous Polarization on the Endurance Fatigue of Si FeFET With Metal/Ferroelectric/Interlayer/Si Gate Structure," *IEEE Trans. Electron Devices*, vol. 70, no. 8, pp. 4055-4061, Aug. 2023, doi: 10.1109/TED.2023.3285715.
- [19] F. Tian, S. Zhao, H. Xu, J. Xiang, T. Li, W. Xiong et al., "Impact of Interlayer and Ferroelectric Materials on Charge Trapping During Endurance Fatigue of FeFET With TiN/Hf_{0.5}Zr_{0.5}O₂/Interlayer/Si (MIFIS) Gate Structure," *IEEE Trans. Electron Devices*, vol. 68, no. 11, pp. 5872-5878, Nov. 2021, doi: 10.1109/TED.2021.3114663.
- [20] Z. Chen, N. Ronchi, A. Walke, K. Banerjee, M. I. Popovici, K. Katcko et al., "Improved MW of IGZO-channel FeFET by Reading Scheme Optimization and Interfacial Engineering," in *Proc. IEEE Int. Memory Workshop (IMW)*, May 2023, pp. 1-4, doi: 10.1109/IMW56887.2023.10145930.
- [21] T. Cui, D. Chen, Y. Dong, Y. Fan, Z. Yao, H. Duan et al., "Can Interface Layer be Really Free for Hf_xZr_{1-x}O₂ Based Ferroelectric Field-Effect Transistors With Oxide Semiconductor Channel?," *IEEE Electron Device Lett.*, vol. 45, no. 3, pp. 368-371, Mar. 2024, doi: 10.1109/LED.2024.3355523.
- [22] Q. Li, S. Wang, Z. Li, X. Hu, Y. Liu, J. Yu et al., "High-performance ferroelectric field-effect transistors with ultra-thin indium tin oxide channels for flexible and transparent electronics," *Nat. Commun.*, vol. 15, no. 1, pp. 2686, Mar. 2024, doi: 10.1038/s41467-024-46878-5.
- [23] P. D. Lomenzo, Q. Takmeel, C. M. Fancher, C. Zhou, N. G. Rudawski, S. Moghaddam et al., "Ferroelectric Si-Doped HfO₂ Device Properties on Highly Doped Germanium," *IEEE Electron Device Lett.*, vol. 36, no. 8, pp. 766-768, Aug. 2015, doi: 10.1109/LED.2015.2445352.
- [24] D. Das, H. Park, Z. Wang, C. Zhang, P. V. Ravindran, C. Park et al., "Experimental demonstration and modeling of a ferroelectric gate stack with a tunnel dielectric insert for NAND applications," in *IEDM Tech. Dig.*, Dec. 2023, pp. 1-4, doi: 10.1109/IEDM45741.2023.10413697.
- [25] C. Y. Chan, K. Y. Chen, H. K. Peng, and Y. H. Wu, "FeFET Memory Featuring Large Memory Window and Robust Endurance of Long-Pulse Cycling by Interface Engineering using High-k AlON," in *Proc. Symp. VLSI Technol.*, Jun. 2020, pp. 1-2, doi: 10.1109/VLSITechnology18217.2020.9265103.
- [26] H.-K. Peng, C.-Y. Chan, K.-Y. Chen, and Y.-H. Wu, "Enabling large memory window and high reliability for FeFET memory by integrating AlON interfacial layer," *Appl. Phys. Lett.*, vol. 118, no. 10, pp. 103503, Mar. 2021, doi: 10.1063/5.0036824.
- [27] A. J. Tan, Y. H. Liao, L. C. Wang, N. Shanker, J. H. Bae, C. Hu et al., "Ferroelectric HfO₂ Memory Transistors with High-κ Interfacial Layer and Write Endurance Exceeding 10¹⁰ Cycles," *IEEE Electron Device Lett.*, vol. 42, no. 7, pp. 994-997, Jul. 2021, doi: 10.1109/LED.2021.3083219.
- [28] A. J. Tan, A. K. Yadav, K. Chatterjee, D. Kwon, S. Kim, C. Hu et al., "A Nitrided Interfacial Oxide for Interface State Improvement in Hafnium Zirconium Oxide-Based Ferroelectric Transistor Technology," *IEEE Electron Device Lett.*, vol. 39, no. 1, pp. 95-98, Jan. 2018, doi: 10.1109/LED.2017.2772791.
- [29] S. Dai, S. Li, S. Xu, F. Tian, J. Chai, J. Duan et al., "Role of Nitrogen in Suppressing Interfacial States Generation and Improving Endurance in Ferroelectric Field-Effect Transistors," *IEEE Trans. Electron Devices*, vol. 71, no. 8, pp. 5081-5088, Sept. 2024, doi: 10.1109/TED.2024.3409203.
- [30] J.-G. Lee, J. Kim, D. I. Suh, I. Kim, G. D. Han, S. W. Ryu et al., "Memory Window Expansion for Ferroelectric FET based Multilevel NVM: Hybrid Solution with Combination of Polarization and Injected Charges," in *Proc. IEEE Int. Memory Workshop (IMW)*, May 2022, pp. 1-4, doi: 10.1109/imw52921.2022.9779292.
- [31] K. Suzuki, K. Sakuma, Y. Yoshimura, R. Ichihara, K. Matsuo, D. Hagishima et al., "High-Endurance FeFET with Metal-Doped Interfacial Layer for Controlled Charge Trapping and Stabilized Polarization," in *IEDM Tech. Dig.*, Dec. 2023, pp. 1-4, doi: 10.1109/IEDM45741.2023.10413699.
- [32] T. Hu, X. Sun, M. Bai, X. Jia, S. Dai, T. Li et al., "Enlargement of Memory Window of Si Channel FeFET by Inserting Al₂O₃ Interlayer on Ferroelectric Hf_{0.5}Zr_{0.5}O₂," *IEEE Electron Device Lett.*, pp. 825-828, May 2024, doi: 10.1109/LED.2024.3381966.
- [33] L. Fernandes, P. V. Ravindran, T. Song, D. Das, C. Park, N. Afroze et al., "Material Choices for Tunnel Dielectric Layer and Gate Blocking Layer for Ferroelectric NAND Applications," *IEEE Electron Device Lett.*, pp. 1-1, Aug. 2024, doi: 10.1109/LED.2024.3437239.
- [34] J. Yang, R. Han, T. Hu, S. Dai, X. Shao, X. Sun et al., "Effect of Nitridation of Bottom Interlayer in FeFETs With the TiN/Al₂O₃/Hf_{0.5}Zr_{0.5}O₂/Bottom Interlayer/Si Substrate Structure," *IEEE Trans. Electron Devices*, pp. 1-7, Oct. 2024, doi: 10.1109/TED.2024.3473889.
- [35] T. Hu, X. Shao, M. Bai, X. Jia, S. Dai, X. Sun et al., "Impact of Top SiO₂ Interlayer Thickness on Memory Window of Si Channel FeFET With TiN/SiO₂/Hf_{0.5}Zr_{0.5}O₂/SiO₂/Si (MIFIS) Gate Structure," *IEEE Trans. Electron Devices*, vol. 71, no. 11, pp. 6698-6705, Nov. 2024, doi: 10.1109/TED.2024.3459873.
- [36] J. Bo, Zurcher, Jones, Gillespie, and Lee, "Computationally Efficient Ferroelectric Capacitor Model For Circuit Simulation," in *Proc. Symp. VLSI Technol.*, Jun. 1997, pp. 141-142, doi: 10.1109/VLSIT.1997.623738.
- [37] X. Shao, J. Chai, F. Tian, S. Zhao, J. Duan, X. Ke et al., "Investigation of Endurance Degradation Mechanism of Si FeFET with HfZrO Ferroelectric by an In Situ V_{th} Measurement," *IEEE Trans. Electron Devices*, vol. 70, no. 6, pp. 3043-3050, Jun. 2023, doi: 10.1109/TED.2023.3265913.
- [38] X. Sun, J. Chai, F. Tian, S. Zhao, J. Duan, J. Xiang et al., "A Physics-Based Model of Charge Trapping Behavior of Si FeFET with Metal/Ferroelectric/Interlayer/Si Structure," *IEEE Trans. Electron Devices*, vol. 70, no. 9, pp. 4641-4646, Sept. 2023, doi: 10.1109/TED.2023.3297082.
- [39] X. Lyu, M. Si, P. R. Shrestha, K. P. Cheung, and P. D. Ye, "First Direct Measurement of Sub-Nanosecond Polarization Switching in Ferroelectric Hafnium Zirconium Oxide," in *IEDM Tech. Dig.*, Dec. 2019, pp. 15.2.1-15.2.4, doi: 10.1109/IEDM19573.2019.8993509.
- [40] J. W. McPherson, "On why dielectric breakdown strength reduces with dielectric thickness," in *Proc. IEEE Int. Rel. Phys. Symp.*, Apr. 2016, pp. 3A-3-1-3A-3-8, doi: 10.1109/IRPS.2016.7574512.